Electronic Materials

IMR KINKEN Research Highlights 2014

Weyl Semimetal Phase in Magnetic Semiconductors

Weyl semimetals are novel topological phases of three-dimensional materials characterized by the existence of a set of linear-dispersive band-touching points called Weyl nodes. We theoretically examined the realization of the Weyl semimetal phase in magnetically doped solid-solution narrow-gap semiconductors with strong spin-orbit interactions, such as Cr-doped $Bi_2(Se_xTe_{1-x})_3$. We computed the spontaneous magnetization of impurities and itinerant electrons and estimated the critical temperature as a function of the concentration of magnetic dopants and the strength of the spin-orbit interactions.

Electric/electronic devices generally utilize the charge of electrons, whereas magnetic devices record information using electron spin. The realization of materials that combine semiconducting behavior with robust magnetism is a central issue in the research field of semiconductor spintronics, and several compound semiconductors that become ferromagnetic when doped with Mn have been discovered. Magnetic order originates from coupling between magnetic element moments, which is mediated by conduction-band electrons or valence-band holes, hence the III-V semiconductors have been studied intensively. The search for new materials is a central goal of this field.

The Weyl semimetals are recently predicted class of novel magnetic materials possessing pseudo-relativistic linear dispersion and magnetic ordering, as shown in Fig. 1(a). Near the band-touching points (or "Weyl points"), the excitations are described by the massless Dirac-Weyl Hamiltonian. Quasiparticles, the Weyl fermions, are assigned a chirality, and the bulk band gap opens only if the two Weyl fermions with opposite chirality meet each other. This topological behavior originates in the non-zero Berry curvature enclosing a Weyl point. Weyl semimetal phases can be regarded as a three-dimensional version of graphene, and a variety of pseudo-relativistic phenomena are expected to emerge. In addition, since spin-orbit coupling is strong in these systems, the spin behavior and electromagnetic field are coupled in nontrivial ways.

We have theoretically estimated the conditions required for realizing the Weyl semimetal phase via doping with magnetic impurities in the Bi_2Se_3 family within the mean-field theory. We found that ferromagnetic ordering in these materials is observed below the critical temperature T_C = 40 K at a magnetic impurity concentration of 5%. This magnetic ordering is introduced by Van Vleck paramagnetism, and thus the critical temperature depends on the strength of the spin-orbit interactions. We confirmed that the critical temperature decreases when the strength of the spin-orbit interactions weakens, and that, as the exchange field increases, the conduction band and the valence band invert. The Weyl semimetal phase is realized as the gapless phase, as shown in Fig. 1(b).

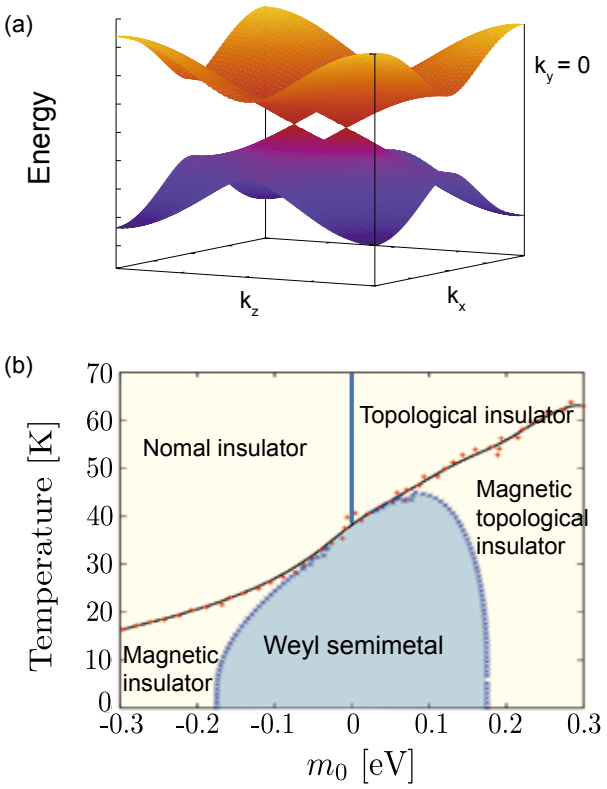

Fig. 1 (a) Energy dispersion in a Weyl semimetal, and (b) obtained phase diagram.

References

[1] D. Kurebayashi and K. Nomura, J. Phys. Soc. Jpn **83**, 063709 (2014).

Keywords: insulator, electrical properties, magnetic properties
Kentaro Nomura (Theory of Solid State Physics Division)
E-mail: nomura@imr.tohoku.ac.jp
URL: http://www-lab.imr.tohoku.ac.jp/~nomura/index.html

Tabletop Pulsed Magnetic Field with 1 ps Time Resolution

A tabletop pulsed magnetic field generator for use in high–time-resolution optical spectroscopy at magnetic fields of 30 T and low temperatures has been developed. Direct optical access was achieved by the design of a sophisticated miniature magnet. The generator provides a time resolution of 1 picosecond, 10 times better than that of conventional measurements.

Optical spectroscopic techniques involving large magnetic fields are important for investigating semiconductors, as well as optical and magnetic compounds. The most important aspects of spectroscopy are the energy resolution and the time resolution. Recent progress in laser technology enables the capture of transient behavior on very short time scales in the ps and fs range. When time-resolved spectroscopy is used alongside an applied magnetic field, however, obtaining high time resolution is difficult because the optical access length is long and complicated.

We have developed a tabletop pulsed magnetic field generator for use with an ultrafast spectrometer in collaboration with Rice University in Houston. IMR's skill in the design of compact, pulsed magnetic field generators was combined with Rice University's sophisticated techniques in ultra-fast spectroscopy, and this collaboration produced a breakthrough in the field of time-resolved spectroscopy at high magnetic fields.

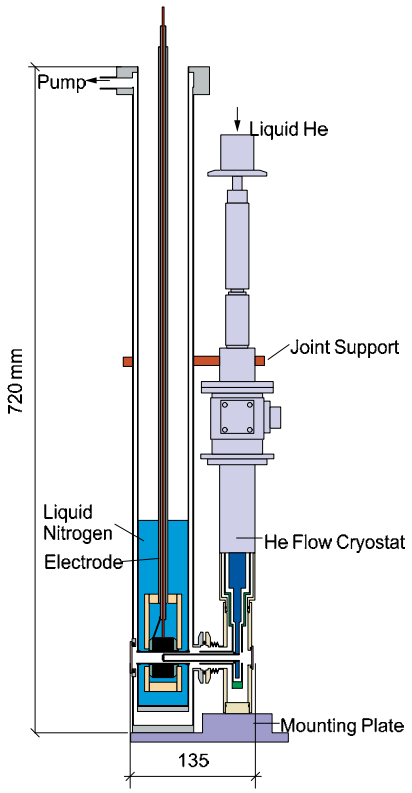

Fig. 1 Schematic of the tabletop spectrometer with a 30 T pulsed magnet.

Fig. 2 Experimental Setup installed at Rice University, Houston. The box in the right is the capacitor bank, and the cylinder in the center is the cryostat with a magnet.

The novel system is so compact that it can be installed on a standard optical bench. Most importantly, the optical access length is as short as 135 mm. Thanks to this short distance between windows, a direct-access geometry is possible. It enables the use a conventional optical setup for ultrafast spectroscopy, and we achieved a time resolution of 1 ps in the photoluminescence measurement of a two-dimensional electron gas in a quantum well.

A magnetic field of 30 T was achieved, and temperatures down to 10 K can be obtained with a conventional He-flow cryostat. These improvements permit such experiments, previously conducted in large-scale facilities, to be performed in normal university laboratories.

Another advantage of this system is the flexibility with respect to upgrades and modifications. In fact, we performed THz-time–domain spectroscopy by extending our table top magnet.

References

[1] G. T. Noe , H. Nojiri, J. Lee, G. L. Woods, J. Léotin, and J. Kono, Rev. Sci. Instrum. **84**, 123906 (2013).

Keywords: photoluminescence, spectroscopy, high magnetic field
Hiroyuki Nojiri (Magnetism Division)
E-mail: nojiri@imr.tohoku.ac.jp
URL: http://www.tohoku.ac.jp/english/2014/01/press20140108-03.html

Discovery of Spin Hall Magnetoresistance

In spintronics, spin currents play a key role in device operation. Here, we report the observation of a novel magnetoresistance effect resulting from a spin current applied across a metal/insulator interface. This spin-current–mediated "spin Hall" magnetoresistance may potentially be used to probe magnetic properties in insulating magnets and to develop spintronic devices.

The resistance of a metallic magnet depends on its magnetization direction, a phenomenon called magnetoresistance (MR). Several types of MR, such as anisotropic, giant, and tunnel MR, are indispensable in present data-storage technologies. For these types of MR to occur, conduction electrons must pass through the magnet. In 2013, we discovered a fundamentally different MR that is caused by nonequilibrium spin accumulation in a metallic Pt film attached to an insulating $Y_3Fe_5O_{12}$ (YIG) magnet [1]. Although conduction electrons in Pt cannot enter YIG, the resistance of the Pt was found to reflect the magnetization direction of the YIG.

The unconventional MR in the Pt/YIG bilayer system originates from concerted actions of the direct and inverse spin Hall effects (SHEs); therefore we call the observed behavior "spin Hall magnetoresistance" (SMR). In the Pt/YIG system, a charge current flowing in Pt induces a spin current $\mathbf{J}_s$ via the SHE (Fig. 1(a)). If the spin polarization $\boldsymbol{\sigma}$ of $\mathbf{J}_s$ and the magnetization $\mathbf{M}$ of the YIG are not collinear, $\mathbf{J}_s$ can propagate across the Pt/YIG interface due to spin transfer torque (Fig. 1(d)). In contrast, if $\boldsymbol{\sigma}$ and $\mathbf{M}$ are collinear, no spin-current transfer across the Pt/YIG interface is possible (Fig. 1(c)). The spin current is then reflected at the interface and converted back into a charge current via the inverse SHE (Fig. 1(b)). Taken together, the magnetization orientation in YIG determines the spin current across the Pt/YIG interface, which in turn affects the magnitude of the charge current in Pt. In this way, the Pt film exhibits MR governed by the magnetic properties of the YIG layer (Fig. 1(e)). SMR can be distinguished from conventional anisotropic MR in ferromagnetic conductors by measuring the magnetic-field-angle dependence of the MR (Fig. 1(f)) [1]. SMR persists even when a Cu layer is inserted between the Pt and the YIG [1]. The experimental results are well explained by a theoretical model [2].

SMR enables remote electrical sensing of the magnetization direction in insulating magnets, implying that the SMR makes the integration of insulating magnets into electronic circuits possible. Since the SMR also provides a powerful and easy method to quantify spin-transport parameters in metals, we anticipate that the SMR will develop into a standard technique for investigating spin-current physics.

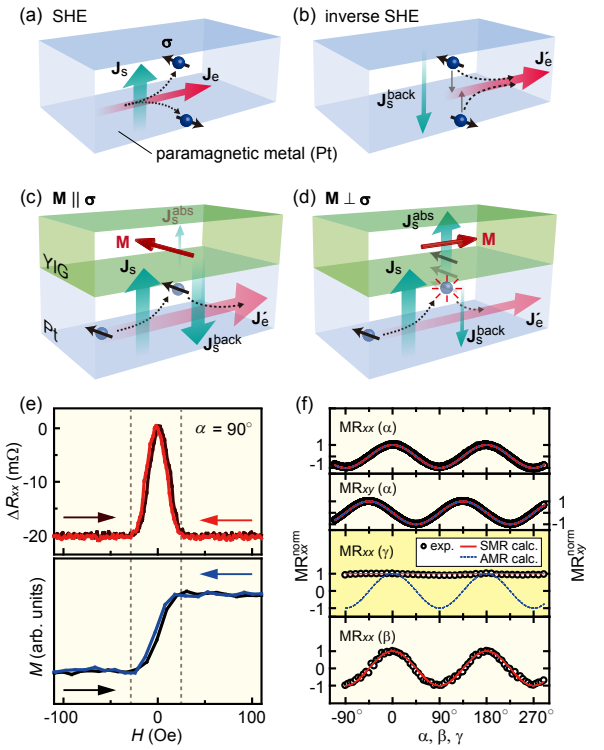

Fig. 1 (a)–(d) Schematic illustrations of the SHE, inverse SHE, and SMR. (e),(f) Magnetic field (H) and magnetic field angle (α, β, γ) dependencies of the SMR in Pt/YIG bilayers [1].

References

[1] H. Nakayama, M. Althammer, Y. T. Chen, K. Uchida, Y. Kajiwara, D. Kikuchi, T. Ohtani, S. Geprägs, M. Opel, S. Takahashi, R. Gross, G. E. W. Bauer, S. T. B. Goennenwein, and E. Saitoh, Phys. Rev. Lett. **110**, 206601 (2013).

[2] Y. T. Chen, S. Takahashi, H. Nakayama, M. Althammer, S. T. B. Goennenwein, E. Saitoh, and G. E. W. Bauer, Phys. Rev. B **87**, 144411 (2013).

Keywords: spintronics, spin transfer, insulator
Eiji Saitoh (Surface and Interface Research Division)
E-mail: eizi@imr.tohoku.ac.jp
URL: http://saitoh.imr.tohoku.ac.jp/

Infrared Blocking or Passing in hand

The field-effect transistor is an effective tool for electrical switching of current flowing at a channel surface by the application of external gate voltages. We recently found that electric-field transistors based on vanadium dioxide exhibit a dramatic change in their "bulk" electronic properties over the electrostatic screening length, potentially leading to novel electronic/optoelectronic device applications. Here, we highlight a new function available with VO_2-based transistors: electrical switching of infrared transmittance without affecting visibility.

VO_2 is a strongly-correlated material with a thermally-induced metal-insulator transition (MIT) above room temperature. A half-filled metallic state is stabilized in a tetragonal form above the transition temperature (T_{MI}), whereas below T_{MI}, vanadium ions are dimerized in a monoclinic form. This structural reorganization at the MIT causes reconstruction of the electronic structure, leading to significant changes both in electrical and optical properties.

We recently reported that the MIT in VO_2 can be electrically switched with an electric double-layer transistor (EDLT) technique [1]. It turned out that the thickness of the electrically induced conducting channel in VO_2-EDLT extends to a length scale of tens of nanometers beyond the fundamental electrostatic screening length. Here, we demonstrate that this new type of field-effect device enabling control of the bulk phase is particularly useful in optoelectronic device applications [2].

The infrared transmittance of VO_2 increases dramatically below T_{MI}, which is known as the thermochromic (TC) effect. We found that VO_2-EDLTs have an electrical switching function for the well-known TC effect. Figure 1 shows the transmission spectra of a 50-nm–thick VO_2 film obtained at 300 K (below T_{MI}) under different applied gate voltages (V_G). A large spectral change is clearly present in the IR region upon gating, indicating a novel electrochromic (EC) effect in VO_2. In contrast, the visible transmittance remains almost unchanged. This large difference in EC sensitivity between the infrared and visible regions has not been achieved in conventional EC devices, making VO_2-EDLTs useful for novel energy-saving smart window applications such as a voltage-tunable transparent heat-cutting filter.

The IR-sensitive EC effect in VO_2 originates from electric-field–induced band reconstruction and subsequent gap closing throughout the entire film, demonstrating the potential value of VO_2-EDLTs as unique multi-functional field-effect devices.

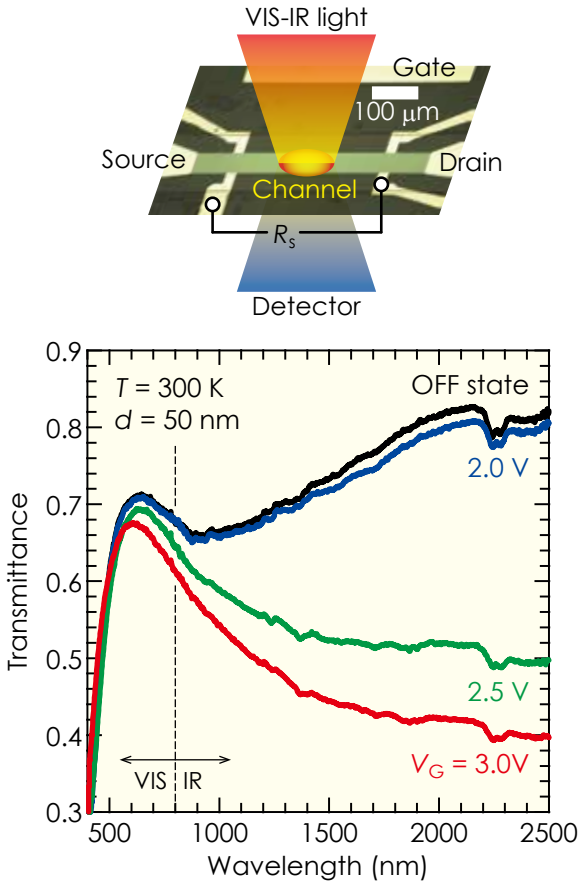

Fig. 1 (top) An optical microscope image of an actual device in the measurement configuration. (bottom) The transmission spectra at 300 K under different applied gate voltages (V_G). The dips around 2250 nm are due to the absorption properties of the ionic liquid molecules used as a gate dielectric layer.

References

[1] M. Nakano, K. Shibuya, D. Okuyama, T. Hatano, S. Ono, M. Kawasaki, Y. Iwasa, and Y. Tokura, Nature **487**, 459 (2012).

[2] M. Nakano, K. Shibuya, N. Ogawa, T. Hatano, M. Kawasaki, Y. Iwasa, and Y. Tokura, Appl. Phys. Lett. **103**, 153503 (2013).

Keywords: oxide, metal-insulator transition, devices
Masaki Nakano (Low Temperature Physics Division)
E-mail: nakano@imr.tohoku.ac.jp
URL: http://mu.imr.tohoku.ac.jp/

Collective Charge Excitation in a Geometrically Frustrated System

We found a characteristic low-energy peak structure in the optical conductivity spectra of a quasi-two–dimensional organic compound with a triangular lattice, θ-(BEDT-TTF)$_2$CsZn(SCN)$_4$, in which competition between two kinds of charge-ordering (CO) patterns leads to a glassy CO state. The observed low-energy peak becomes significant as the temperature drops and shifts to much lower frequencies for a single polarization direction, which suggests that the low-energy peak originates from collective excitation related to the glassy electronic state.

Charge ordering (CO) is one of the most striking manifestations of Coulomb interactions in strongly correlated electron systems. It is well known that Wigner-type CO often emerges in quarter-filled electron systems. In this type of CO, the off-site Coulomb interaction plays an important role in the formation of localized electrons, mostly leading to long-range CO. Recently, however, in geometrically frustrated systems, short-range/glassy CO states without any long-range order have been observed.

Here we report on the characteristic low-energy peak structure observed in the optical conductivity spectra of θ-(BEDT-TTF)$_2$CsZn(SCN)$_4$ (or "θ-CsZn") [1]. The BEDT-TTF molecules of this salt form a 2D conducting plane with a triangular lattice, where the ratio of the nearest-neighbor Coulomb repulsions V_c and V_p is close to unity (see the inset of Fig. 1). Due to the geometrical frustration, θ-CsZn exhibits no clear long-range CO, but rather the coexistence of two kinds of short-range CO (or a "glassy" CO state). Figure 1 shows the optical conductivity spectra of θ-CsZn. When the temperature is lowered, the broad band located around 300 cm^{-1} at room temperature shifts to lower frequencies and becomes sharper, especially for ***E*//*a***. The central frequency of the low-energy peak exhibits a large shift from 300 to 100 cm^{-1} for ***E*//*a***, whereas for ***E*//*c*** it shows only a slight change. This unidirectional behavior of L_{low} is in a sharp contrast with the other two broad electronic transitions, L_{middle} and L_{high}. Recent theoretical calculations including the full long-range Coulomb interactions predict the manifestation of a collective excitation. According to this model, in the vicinity of CO, the electrons can resonate between nearly-degenerate energy states, which form a collective excitation that can coherently propagate at long distances. In θ-CsZn, a short-range CO with a relatively long-period 3 x 3 pattern caused by the long-range Coulomb interactions has been observed; this is considered to be the origin of the glassy CO state. Therefore, the low-energy peak can be attributed to a collective excitation originating from the short-range 3 x 3 CO.

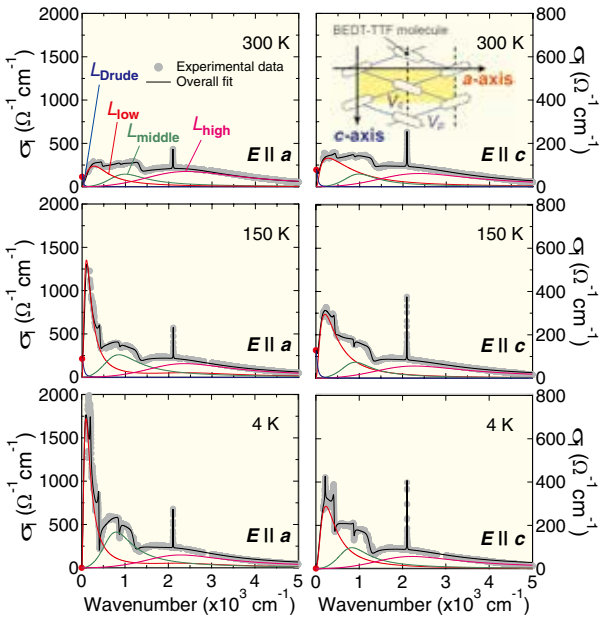

Fig. 1 Optical conductivity spectra of θ-CsZn at 4, 150, and 300 K for ***E*ll*a*** and ***E*ll*c***. The red circles at ω = 0 indicate the dc conductivity. The black lines represent the overall fit. The blue, red, green, and magenta lines correspond to the Drude term, L_{low}, L_{middle}, and L_{high} bands, respectively. The inset shows a schematic of the arrangement of BEDT-TTF molecules in the θ-type salts.

The present results shed light on the low-energy excitations in the glassy electronic state, where the charge degrees of freedom remain at low temperatures.

References

[1] K. Hashimoto, S.C. Zhan, R. Kobayashi, S. Iguchi, N. Yoneyama, T. Moriwaki, Y. Ikemoto, and T. Sasaki, Phys. Rev. B **89**, 085107 (2014).

Keywords: organic, glass-forming ability, optical properties
Kenichiro Hashimoto and Takahiko Sasaki (Low Temperature Condensed State Physics Division)
E-mail: hashimoto@imr.tohoku.ac.jp
URL: http://cond-phys.imr.tohoku.ac.jp/

Thermal Double Donors: Defect Reactions in Ge

Elucidation of defect formation and dissociation in crystals is essential to develop functional devices based on crystalline materials. Thermal double donors (TDDs) are typical defects in heat-treated Si and Ge formed by aggregation of interstitially dissolved oxygen (O_i) atoms. We recently clarified the formation and rate-controlling mechanisms of TDDs in high-quality Ge crystals.

A thermal double donor (TDD) is an O_i-based defect that develops upon heat-treatment at temperature of 300–450°C in Si and Ge. Elucidation of the formation mechanism and properties of TDDs is a long-term topic in defect study of semiconductors since TDDs have a critical influence on device functionality. Also, the rate-controlling mechanism is interesting as aggregation of O_is in terms of solid-state reactions. The research developed mainly in Si, and at present, the atomic structure of TDDs is supposed to be a pair of atomic chains of O_is, called the O_n-2NN model [1]. Contrarily, TDDs in Ge are far less known due to material limitations that the concentration of O_is is generally low in Ge. Establishing structure and formation mechanism of TDDs in Ge besides in Si is important to general defect science.

We recently succeeded in clarifying the formation and growth of TDDs in O_i-rich Ge crystals due to heat treatments at temperatures of 300–500˚C for durations up to 3500 h [2,3]. Ge crystals with O_i concentration [O_i] of 4–5 × 10^{17} cm^{-3} were grown by an advanced Czochralski method adopting liquid-B_2O_3 encapsulation and GeO_2 powder doping [4]. The variation in [O_i] was evaluated using infrared absorption at room temperature (RT), and TDD concentration [TDD] was measured by Hall-effect study at RT.

The absorption peak at 855 cm^{-1} related to O_i shrank and the peak at 780 cm^{-1} related to TDDs developed with heat treatments at 300–450˚C. In the heat treatments, the [O_i]s evaluated with the peak intensity saturated, corresponding to the solubility limit at the temperature. TDD formation was confirmed electrically that [TDD] was ~5 × 10^{16} cm^{-3} (Fig. 1). From a kinematic analysis of the reduction in [O_i], two stages for TDD formation were proposed: In the early stage of heat treatment, an oxygen atom is captured by another oxygen atom to form an O_{dimer}. The merge reaction of two O_is is dominant as a nuclei of TDDs. In the prolonged stage, a TDD, generated from an O_{dimer}, develops through additional absorption of O_i via diffusion, indicating the O_n-2NN model (Fig. 2), in a balance

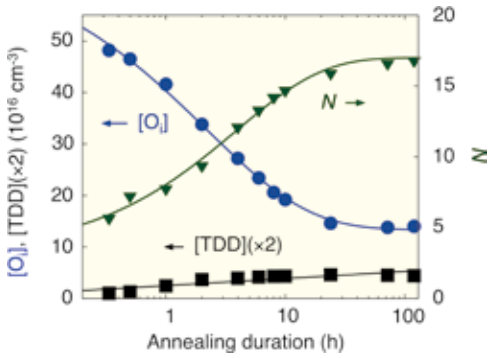

Fig. 1. Variation of [O_i], [TDD], and average number N of oxygen atoms involved in each TDD with annealing duration at 400˚C.

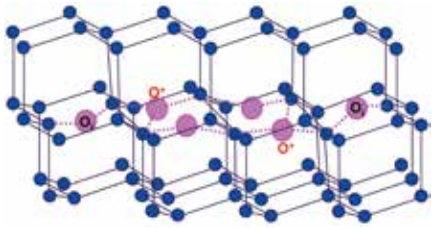

Fig. 2. O_n-2NN model of TDDs. Red and blue balls are O and Ge atoms, respectively.

with their dissociation at elevated temperatures. The evaluated activation energies of both reactions were 1.7 and 2.0 eV, showing that O_i diffusion is rate-controlling. The number of O_i involved into a TDD is 16–19 in the thermal equilibrium state at 325–400 °C.

References

[1] L. I. Murin, J. L. Lindström, V. P. Markevich, T. Hallberg, V. V. Litvinov, J. Coutinho, R. Jones, P. R. Briddon, and S. Öberg, Physica B **308-310**, 29 (2001).

[2] K. Inoue, T. Taishi, Y. Tokumoto, Y. Murao, K. Kutsukake, Y. Ohno, M. Suezawa, and I. Yonenaga, J. Appl. Phys. **113**, 073501 (2013).

[3] K. Inoue, T. Taishi, Y. MUrao, Y. Tokumoto, K. Kutsukake, Y. Ohno, and I. Yonenaga, J. Phys. Soc. Conf. Proc. **1**, 012082 (2014).

[4] T. Taishi, H.Ise, Y. Murao, T.Ohsawa, M. Suezawa, Y. Tokumoto, Y. Ohno, K. Hoshikawa, and I. Yonenaga, J. Cryst. Growth **312**, 2783 (2010).

Keywords: defects, kinetics, semiconducting
Ichiro Yonenaga (Physics of Crystal Defects Division)
E-mail: yonenaga@imr.tohoku.ac.jp
URL: http://lab-defects.imr.tohoku.ac.jp

Changing the Polarity of Our Thinking: Full-Color Emission from Nitrogen-Polarity InGaN LEDs

The deterioration of crystal quality by spinodal decomposition and strain relaxation, which hinders the uniform incorporation of immiscible indium into InGaN alloys, was successfully inhibited by flipping the crystallographic orientations of InGaN alloys from a widespread group-III (+*c*) polarity to a novel nitrogen (–*c*) polarity counterpart. As a consequence of the efficient reduction of the bandgap energy, full-color light-emitting diodes were obtained.

The realization of full-color light-emitting diodes (LEDs) composed of InGaN/GaN quantum wells requires higher indium-content InGaN alloys with red emission. This has never achieved due to the high immiscibility of In, the huge strain accumulated at the heterointerfaces, and the catastrophic degradation of the crystal quality during metal-organic vapor phase epitaxy (MOVPE) along the usual crystallographic orientation of group-III (+*c*) polarity (Fig. 1(a)). We reversed the directionality of the entire structure in order to overcome this issue because InGaN growth along the nitrogen (–*c*) polarity orientation (Fig. 1(b)) was reported to be advantageous for the incorporation of In. Additionally, based on the drastically modified growth mode and the strain relaxation mechanism anticipated from the difference in the chemical stability of this polar surface, we optimized the basic growth conditions [1].

All of the LED structures were fabricated by MOVPE on *c*-plane sapphire substrates with a miscut angle of 0.8° toward the *m*-direction. Growth was initiated by nitridation of the sapphire surface in order to establish the crystallographic orientation of nitride films as the –*c* polarity. After the sequential stacking of a low-temperature GaN buffer layer, undoped GaN, GaN:Si and five-period of InGaN/GaN multiple quantum wells (MQWs) were grown, followed by the depositions of a GaN layer and a GaN:Mg contact layer. The optimum growth conditions and structures of MQWs, such as the mixture ratios of source and carrier gases ratios and the well and barrier thicknesses, were explored utilizing standard structural investigation techniques such as high-resolution X-ray diffraction, atomic-force microscopy and electron backscatter diffraction, as well as photoluminescence measurements. It was found that the introduction of hydrogen gas and the reduction of V/III precursor supply ratios during the growth of the GaN barrier layer are important in maintaining the flatness of the interface and suppressing metastable phase

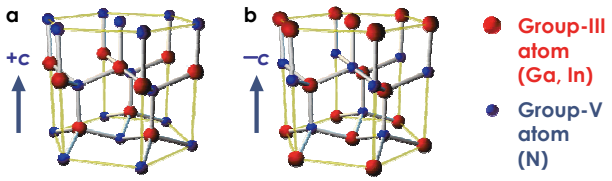

Fig. 1 Orientation of InGaN with (a) group-III (+*c*) and (b) nitrogen (–*c*) polarities.

Fig. 2 Full-color RGB emission from $In_xGa_{1-x}N$/ GaN MQW LEDs with different indium contents *x* of (a) 0.40, (b) 0.29, and (c) 0.17.

inclusion. We found that the indium content within the InGaN well layer was increased by intentionally lowering the growth temperature from 880 to 790 °C. The samples were annealed in air at 750 °C for 5 minutes to activate the Mg acceptors within the contact layer, and the electroluminescence (EL) was measured at room temperature.

Figure 2 shows the EL image of nitrogen-polarity InGaN/GaN MQW LEDs with estimated indium contents *x* of 0.40, 0.29 and 0.17. After optimizing the multiple growth parameters, a bright red emission was achieved.

This change in the way of thinking, a simple inversion of the crystallographic orientation of the device, lead to a long sought-after result: the accessibility of the entire visible spectral range by nitride-based LEDs.

References

[1] T. Tanikawa, K. Shojiki, J. H. Choi, T. Aisaka, T. Kimura, S. Kuboya, T. Hanada, R. Katayama, and T. Matsuoka, Jpn. J. Appl. Phys. **53**, 05FL05 (2014).

Keywords: optoelectronic, semiconducting, nitride
Takashi Matsuoka (Physics of Electronic Materials Division)
E-mail: matsuoka@imr.tohoku.ac.jp
URL: http://www.matsuoka-lab.imr.tohoku.ac.jp/

A Unique Way to Create Carriers in Donor/Acceptor Chains

A material containing electron-donor/acceptor metal-complexes is a good platform for the synergistic control of electron transport and spin ordering. However, it is not easy to create or control electronic carriers that can freely move in low-dimensional D/A frameworks. We have recently found that doping a redox-inert (insulator) element into a D^+A^- ionic chain in place of a neutral D increases the conductivity.

The control of charge transfer and electron transfer in multidimensional frameworks could be an efficient way to design electronically/magnetically functional materials. One candidate class of materials for achieving such control is those consisting of electron-donor/acceptor metal-complex assemblies in which strongly correlated multiple *d*-orbital spins are available, as well as electron transport through the frameworks [1].

To control electron transport in a one-dimensional DA chain, we propose a unique idea: the doping of a redox-inert (insulator) dopant (P) into a D^+A^- chain in place of a neutral D. This doping creates mixed valence A^0/A^- domains between P units, $P–(D^+A^-)_nA^0–P$, where *n* is directly dependent on the dopant ratio, and charge transfer through the P units leads to electron transport along the framework (Fig. 1 (a)). This hypothesis was demonstrated in an ionic D^+A^- chain derived from the reaction of a paddlewheel $[Ru_2^{II,II}]$ complex with an organic acceptor (TCNQ derivative) by doping a redox-inert $[Rh_2^{II,II}]$ unit.

Figure 1 (b) shows the dc resistivity (ρ_{dc}) of all compounds as a function of temperature, as measured using a two-probe dc-current technique on single crystals (parallel to the chain). All compounds exhibit typical semiconductor behavior, but ρ_{dc} tends to decrease exponentially with increasing amount of $[Rh_2^{II,II}]$ dopant. Since the $[Rh_2^{II,II}]$ unit is relatively redox-inert and the $[Rh_2^{II,II}]$-pure chain is an insulator ($\rho_{dc} > 10^{10}$ Ω cm), the charge carriers must be provided by the mixed valence A^0/A^- sets in domains and transferred through the $[Rh_2^{II,II}]$ units, demonstrating a unique way to rationally create a hole in an ionic D^+A^- chain.

Note that the doping of diamagnetic $[Rh_2^{II,II}]$ also tunes the magnetic transition temperatures, because the domain size in a chain (i.e., the magnitude of the dipole) made by dopants is a key to controlling the interchain interaction associated with the bulk magnetism [3].

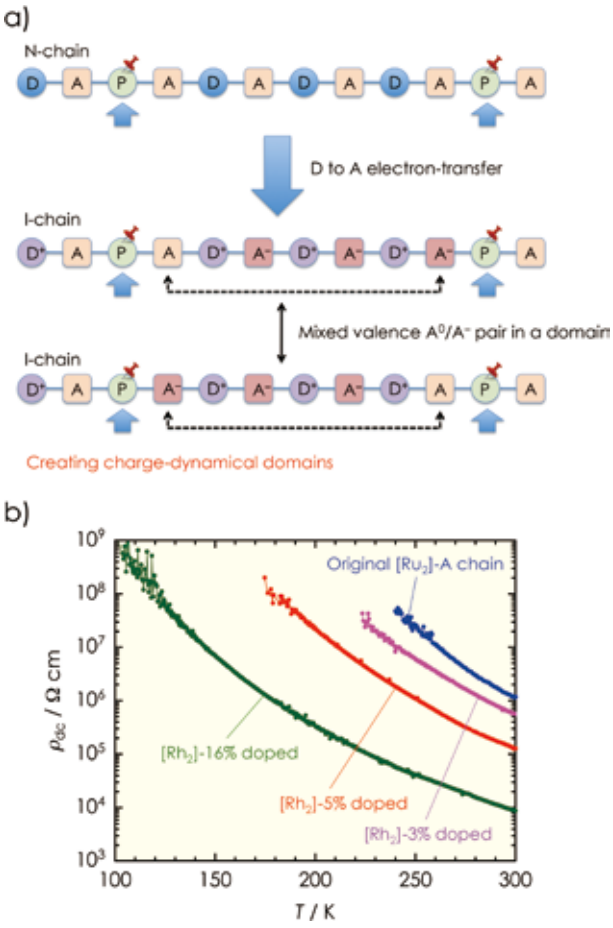

Fig. 1 (a) Schematic representations of charge arrangements in a P-doped D^+A^- ionic chain. (b) Temperature dependence of ρ_{dc} measured on single crystals using a two-probe dc-current technique.

References

[1] H. Miyasaka, *Acc. Chem. Res.* **46**, 248 (2013).
[2] M. Nishio, N. Hoshino, W. Kosaka, T. Akutagawa, and H. Miyasaka, *J. Am. Chem. Soc.* **135**, 17715 (2013).
[3] M. Nisho and H. Miyasaka, *Inorg. Chem.* **53**, 4716 (2014).

Keywords: chemical substitution, electrical properties, magnetic properties
Hitoshi Miyasaka (Solid-State Metal-Complex Chemistry Division)
E-mail: miyasaka@imr.tohoku.ac.jp
URL: http://www.miyasaka-lab.imr.tohoku.ac.jp

Artificial Fabrication of $L1_0$-FeNi with High Magnetic Anisotropy and Low Magnetization Damping

Trends of elements strategy have led to an increased demand for hard magnetic alloys or compounds that do not contain rare earths or noble metals, key materials not only in permanent magnets but also next-generation magnetic recording media and magnetic memories. $L1_0$-FeNi is a candidate with high uniaxial magnetic anisotropy but without a rare earth or noble metal component. In this study, we fabricated $L1_0$-FeNi thin films by depositing Fe and Ni monatomic layers alternately and investigated the magnetic properties, including the magnetization dynamics. Our experiment shows that $L1_0$-FeNi possesses both high magnetic anisotropy and low magnetization damping.

Hard magnetic materials with large magnetic anisotropy typically contain rare earth and/or noble metal elements. Because of the shortage of these elements in the environment, alternative hard magnet materials without these elements are desired. $L1_0$-FeNi shows promise as one of the alternatives since it exhibits high uniaxial magnetic anisotropy (K_u). However, its low order-disorder transition temperature, which gives rise to slow atomic diffusion, results in difficulties in $L1_0$ ordering with conventional bulk or thin-film preparation processes. Thanks to well-controlled deposition techniques in which monatomic Ni and Fe layers are alternately deposited, we successfully prepared $L1_0$-FeNi thin films with relatively high K_u [1].

In this study, we carried out a systematic study on the composition dependence of the magnetic anisotropy in $L1_0$-FeNi. All thin films were prepared using an ultrahigh-vacuum–compatible molecular beam epitaxy system. Monolayers (MLs) of Fe and Ni were alternately deposited on a $Au_6Cu_{51}Ni_{43}$ buffer. In order to examine the composition dependence of the magnetic properties, FeNi films with different compositions were prepared by alternately depositing $(1 + x)$ MLs of Ni and $(1 - x)$ MLs of Fe. The experimental results indicated that K_u and the saturation magnetization showed maxima at $Fe_{60}Ni_{40}$, while the highest $L1_0$ ordering parameter was obtained for $Fe_{50}Ni_{50}$ [2]. Therefore, we found that enrichment of Fe was effective in enhancing K_u.

We also studied the magnetization dynamics for $L1_0$-FeNi and disordered FeNi in order to understand the relationship between K_u and the magnetization damping constant (α). Figure 1 shows the dependence of α on the external magnetic field (H) for $L1_0$-FeNi and disordered FeNi, which was evaluated using the time-resolved magneto-optical Kerr effect. As H increased, α for the $L1_0$-FeNi drastically decreased to 0.013 ± 0.001. On the other hand, the disordered FeNi showed no remarkable dependence of α on H, and α = 0.009 ± 0.002 was obtained. This suggests that the extrinsic contributions enhancing α are suppressed in $L1_0$-FeNi by the application of a large H. An important finding is that α for the $L1_0$-FeNi is as small as that of the disordered FeNi, even though the $L1_0$-FeNi has a relatively high K_u. This means that $L1_0$-FeNi is a promising material possessing high K_u and low α [3].

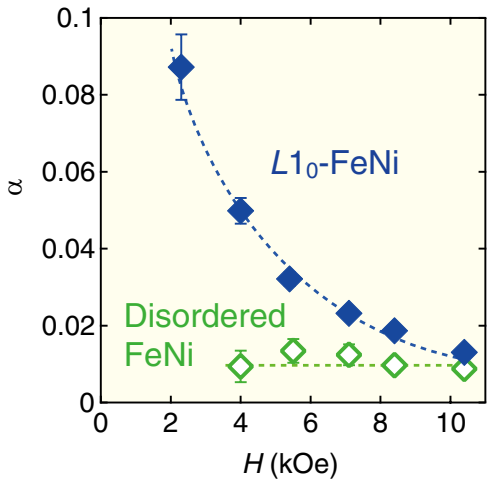

Fig. 1 H-dependence of the magnetization damping constant (α) for $L1_0$-FeNi and disordered FeNi.

References

[1] T. Kojima, M. Mizuguchi, T. Koganezawa, K. Osaka, M. Kotsugi, and K.Takanashi, Jpn. J. Appl. Phys. **51**, 010204 (2012).

[2] T. Kojima, M. Ogiwara, M. Mizuguchi, M. Kotsugi, T. Koganezawa, T. Ohtsuki, T. Y. Tashiro, and K. Takanashi, J. Phys.: Condens. Matter. **26**, 064207 (2014).

[3] M. Ogiwara, S. Iihama, T. Seki, T. Kojima, S. Mizukami, M. Mizuguchi, and K. Takanashi, Appl. Phys. Lett. **103**, 242409 (2013).

Keywords: molecular beam epitaxy, magnetic properties, spintronics
Koki Takanashi (Magnetic Materials Division)
E-mail: koki@imr.tohoku.ac.jp
URL: http://magmatelab.imr.tohoku.ac.jp/

Degrees-of-Freedom Model at a Crystal Site That Could Save Time and Money when Designing a New Crystal Structure

A model of the degrees of freedom at a crystal site is introduced through an example application to evaluate the defect structure of $LiNbO_3$. The degrees of freedom are obtained by subtracting the number of constraints from the number of parameters. The model is useful for narrowing down the possible crystal structures in materials consisting of multiple elements.

When constructing a new crystal structure [1], it is important to determine the element occupying each crystal site. These elements include constituent cations, impurity ions, anti-site defects, and vacancies. The possible occupant of a site is examined by considering the associated degrees of freedom, and we will apply a new concept of the degrees of freedom at a crystal site to an unsolved problem concerning the crystal structure of $LiNbO_3$.

The degrees of freedom are obtained by subtracting the number of constraints from the number of parameters. The number of parameters at a site is the number of elements, while at least three types of constraints are considered, as follows:

(1) Mass conservation holds at each site.
(2) If an element is present at multiple sites in a crystal, its chemical potentials at those sites are equal.
(3) The vacancy population is calculated in such a way that overall charge neutrality is maintained in the bulk crystal.

The additional constraints will be found as needed.

The location of vacancies in congruent $LiNbO_3$ (c-LN), i.e., whether the vacancy is present at a Li site or Nb site, has been an issue for a long time since it was invented more than half a century ago at Bell Labs. A tremendous amount of time and money has spent on this issue. Experimentally, many kinds of spectroscopic techniques have been applied, though they have not been successful in presenting the complete structure analysis.

Here, we applied a new concept of the degrees of freedom at a crystal site and put an end to this issue. Figure 1(a) shows the site structure where the vacancy is located at the Li site. The degrees of freedom at both the Li and Nb sites are zero, which is fine for constructing a structure. In contrast, the presence of a vacancy at the Nb site in Fig. 1(b) leads to –1 degree of freedom at the Nb site. This situation occurs because the Nb is present in both Nb and Li sites and they are in equilibrium, which yields one more constraint. The negative degrees of freedom do not accept such a crystal structure.

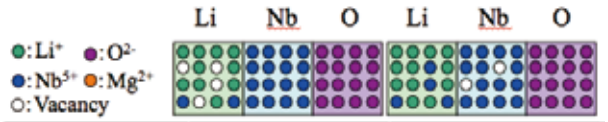

	c-LN (V in Li site)	c-LN (V in Nb site)
Elements in Li site	Li, Nb, V	Li, Nb
Elements in Nb site	Nb	Nb, V
Elements in O site	O	O
No of parameters in Li site	3	2
Constraints in Li site	• Mass conservation • μNb(Li)= μNb(Nb) • V charge balance	• Mass conservation • μNb(Li)= μNb(Nb)
No of parameters in Nb site	1	2
Constraints in Nb site	• μNb(Li)= μNb(Nb)	• Mass conservation • μNb(Li)= μNb(Nb) • V charge balance
Degrees of freedom	0 (Li site), 0 (Nb site)	0 (Li site), -1 (Nb site)

Fig. 1 Two possible vacancy configurations in congruent $LiNbO_3$: (a) vacancies at Li sites and (b) vacancies at Nb sites.

This model of the degrees of freedom is based on thermodynamic principles and is a powerful tool for designing a new crystal structure.

References

[1] S. Fujii, S. Uda, K. Maeda, J. Nozawa, H. Koizumi, K. Fujiwara, and T. Kajigaya, J. Cryst. Growth **383**, 63 (2013).

Keywords: crystal structure, degrees of freedom, vacancy
Satoshi Uda (Crystal Chemistry Division)
E-mail: uda@imr.tohoku.ac.jp
URL: http://www.uda-lab.imr.tohoku.ac.jp/index.html

Development of a High-performance Ce-doped $(La,Gd)_2Si_2O_7$ Scintillator (Ce:La-GPS)

A new La-admixed Ce-doped $(La,Gd)_2Si_2O_7$ (Ce:La-GPS) scintillator has been developed. This material exhibits a high light yield of 40000 photons per MeV and a relatively fast scintillation response with a decay time of around 40–50 ns. In addition, the material has a potential to find application in Compton imaging or oil-well logging.

Scintillation detectors are used for detection of ionizing radiation such as X-rays, gamma rays or elementary particles. They consist of a scintillation material, which converts the energy of the ionizing radiation into visible or UV light, and a photodetector, which detects the emitted visible/UV light. Scintillation detectors are used in X-ray computed tomography, positron emission tomography and other medical imaging techniques, high energy and nuclear physics applications, and natural resource surveys.

Ce-doped Gd_2SiO_5 gadolinium silicate single crystals (Ce:GSO) are widely used scintillation materials. Recently, promising scintillation parameters have been discovered for Ce-doped pyrosilicate crystals such as $Gd_2Si_2O_7$ that are mechanically stable and non-hygroscopic. However, incongruent melting of $Gd_2Si_2O_7$ prevents the growth of high quality crystals from the melt. It has been shown that the pyrosilicate phase can be stabilized by heavy Ce-doping (10 mol%); however, a high concentration of the Ce^{3+} luminescent ions leads to concentration quenching and degradation of the scintillation performance. As the ionic radius of non-luminescent La^{3+} ions is close to that of Ce^{3+} ions, we were able to demonstrate that the pyrosilicate phase can be stabilized by La^{3+}, maintaining the Ce^{3+} concentration as low as 1 mol%. Promising scintillation parameters of $(Ce_{0.01}Gd_{0.90}La_{0.09})_2Si_2O_7$ (Ce:La-GPS) single crystals, such as a high light yield of 36000 photons per 1 MeV of absorbed energy and a scintillation decay of around 46 ns, have been demonstrated [1]. Also, this material has no intrinsic radioactivity which would lead to a background signal increase, so it can be applied in, for example, gamma-ray astronomy or Compton imaging. (The latter technique can be used also for radioactive contamination mapping.)

A high energy resolution of 5% for 662 keV gamma rays and the emission wavelength at 390 nm (Fig. 1) favorably placed in the sensitivity region of contemporary photomultipliers and some silicon avalanche photodiodes (Si-APD) are the other significant merits of this material. We have also demonstrated an even higher light yield value of

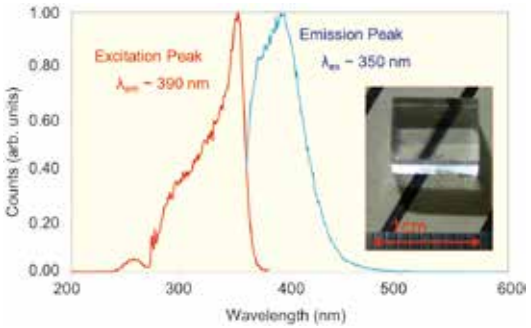

Fig. 1 Photoluminescence excitation and emission spectra of the Ce:La-GPS single crystal. A photo of the as-grown crystal is shown in the inset.

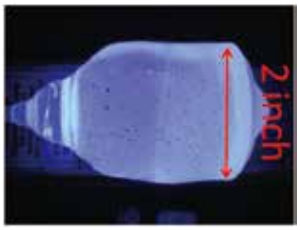

Fig. 2 2-inch La-GPS single crystal (as grown)

41000 photons per MeV for crystals grown using by the floating-zone method when coupled with a Si-APD [2]. Another advantage of this material is that its light yield remains nearly constant up to temperatures around 150°C. The thermal stability of the material parameters and mechanical hardness make it suitable for applications such as geological survey or oil-well logging, where the material is often exposed to harsh conditions and high temperatures deep below the Earth's surface. Our future research will consist of further development of this promising material, including the optimization of its composition and growth conditions. The recently grown 2-inch bulk single crystal is shown in Fig. 2.

References

[1] A. Suzuki, S. Kurosawa, T. Shishido, J. Pejchal, Y. Yokota, Y. Futami, and A. Yoshikawa, Appl. Phys. Express **5**, 102601 (2012).
[2] S. Kurosawa, T. Shishido, A. Suzuki, J. Pejchal, Y. Yokota, and A. Yoshikawa, Nucl. Inst. Meth. Phys. Res. A **744**, 30 (2014).

Keywords: crystal growth, luminescence, lanthanide
Akira Yoshikawa (Advanced Crystal Engineering Laboratory)
E-mail: yoshikawa@imr.tohoku.ac.jp
URL: http://yoshikawa-lab.imr.tohoku.ac.jp/index-e.html

Incommensurate Magnetic Ordering Triggered by Superconductivity

We discovered an incommensurate magnetic ordering inside the superconducting phase in a rare-earth heavy-fermion compound. This so-called "Q-phase" was found to be related to the anisotropic superconducting gap. This finding will shed light on the mechanisms of superconductivity and magnetism.

The interplay between magnetism and superconductivity, such as the coexistence of ferromagnetism and superconductivity [1], is an essential topic of modern condensed matter physics. In a conventional superconductor, a full gap opens at the Fermi surface at the superconducting transition temperature and ordering involving the same electrons occurs inside the superconducting phase. Unconventional superconductors with a finite electronic density of states at the Fermi levels arising from the nodes that characterize their superconducting gap allow for such a possibility. This situation, where magnetic ordering occurs below a superconducting ordering, is nonetheless experimentally rare.

In $CeCoIn_5$, a so-called "heavy fermion system" where 4f electrons are subject to strong interactions, a superconducting state appears below 2.3 K. Under a magnetic field applied in the basal plane of the tetragonal structure, superconductivity is suppressed at the upper critical field H_{c2} = 11.4 T by a mechanism that acts on the spin Cooper pairs. Another important effect is the occurrence of a magnetic-field–induced incommensurate magnetic ordering in the vicinity of H_{c2}. This order disappears above H_{c2}, which indicates a collaborative effect between magnetism and superconductivity. This unique state of matter, named the "Q-phase," has led to a wealth of theoretical works pointing to many possible scenarios.

We studied a sample of $CeCoIn_5$ with a small Nd substitution (5%) [2]. This material realizes the peculiar experimental situation described above where the antiferromagnetic ordering temperature (0.9 K) is lower than the superconducting transition temperature (1.85 K), as shown in Fig. 1(a). Surprisingly, the same incommensurate magnetic ordering as in the pure $CeCoIn_5$ compound under an applied magnetic field, the Q-phase, was observed in the neutron scattering experiments (see Fig. 1(b)). Hence, the magnetic field is not an essential ingredient for realizing this peculiar state, and this requires sharpening theoretical scenarios

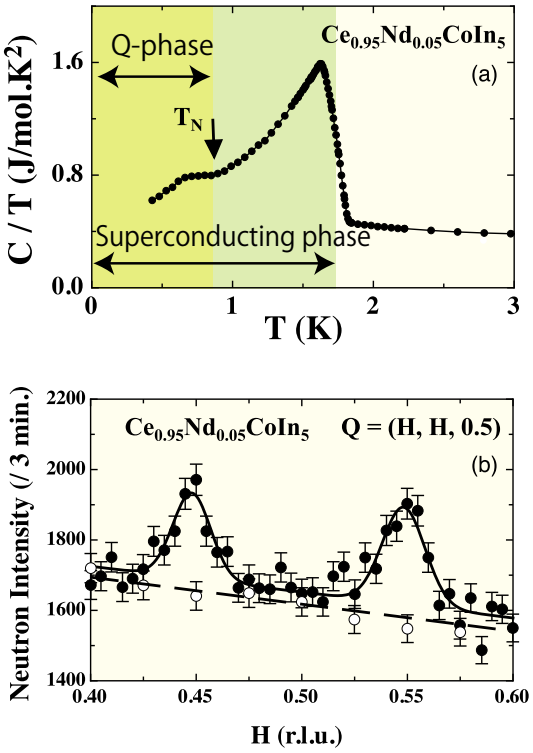

Fig. 1 (a) Temperature dependence of the specific heat of $(Ce_{0.95}Nd_{0.05})CoIn_5$. The antiferromagnetic ordering temperature (0.9 K) is lower than the superconducting transition temperature (1.85 K). (b) Q-scan along the [H,H,0.5] direction in the neutron scattering experiments; the incommensurate scattering vector Q was identified.

for this phase. However, it also shows that superconductivity plays a key role in the realization of this peculiar magnetic ordering. One possibility is that the nodes in the superconducting gap favor the nesting conditions needed to realize an incommensurate magnetic ordering. This work was done in collaboration with S. Raymond in CEA-Grenoble.

References

[1] D. Aoki and J. Flouquet, J. Phys. Soc. Jpn. 81 (2012) 011003.
[2] S. Raymond, S. M. Ramos, D. Aoki, G. Knebel, V.P. Mineev, and G. Lapertot, J. Phys. Soc. Jpn. 83 (2014) 013707.

Keywords: superconducting, Fermi surface, heavy fermion
Dai Aoki (Actinide Materials Science Division)
E-mail: aoki@imr.tohoku.ac.jp
URL: http://actinide.imr.tohoku.ac.jp

Z-contrast STEM Imaging of Long-Range Ordered Structures in Magnetic Nanoparticles

The atomic structures of epitaxial $L1_0$ CoPt nanoparticles (NPs) were imaged using chemically sensitive high-angle annular dark-field scanning transmission electron microscopy (HAADF-STEM). It was found that the (001) facets of the multi-variant NPs are terminated by Co atoms rather than by Pt atoms in contrast to theoretical predictions.

CoPt alloy nanoparticles (NPs) with the $L1_0$-type ordered structure are candidate materials for use in future ultrahigh-density magnetic storage media. The magnetocrystalline anisotropy energy of the NPs depends on the long-range order (LRO); atomic ordering and the stability of the ordered phase are key issues in the realization of excellent hard magnetic properties [1]. To extract chemical information related to the LRO with atomic resolution, atomic-number (*Z*) contrast imaging by high-angle annular dark-field scanning transmission electron microscopy (HAADF-STEM) is quite useful [2, 3].

CoPt NPs were fabricated by sequential electron-beam deposition of Pt, Co, and Al_2O_3 onto NaCl(001) substrates followed by post-deposition annealing [3].

Figure 1(a) shows a HAADF-STEM image of a single crystal $L1_0$ CoPt NP. The two types of bright dots, strong and weak, correspond to Pt and Co atomic columns, respectively, due to the alternate stacking of Co and Pt. The image contrast of the (110) superlattice is lower in the peripheral regions than in the center of the NP. To clarify this contrast variation, we simulated the HAADF-STEM images using a model cluster.

Figure 2(a) shows a structure model and a simulated image of a fully ordered CoPt NP. The contrast variation from the particle center to the {111} or {100} facets is reproduced in the simulated image of the fully ordered NP. Figure 2(b) shows intensity profiles of the simulated images. Intensity degradation towards {111} facet (B-B') is prominent compared to that of {100} (A-A'). Thus, the image simulation revealed that the experimentally observed degradation in image contrast can be attributed to the thickness reduction in the peripheral region due to particle shape rather than possible variation of the LRO.

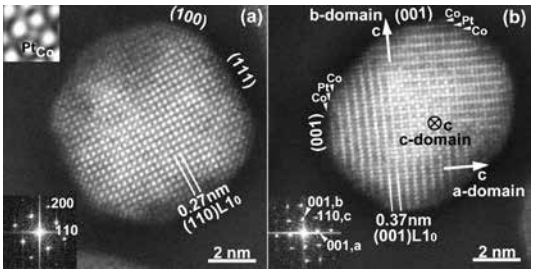

Fig. 1 HAADF-STEM images of $L1_0$-CoPt NPs after annealing at (a) 973 K for 6 ks and (b) 873K for 36 ks.

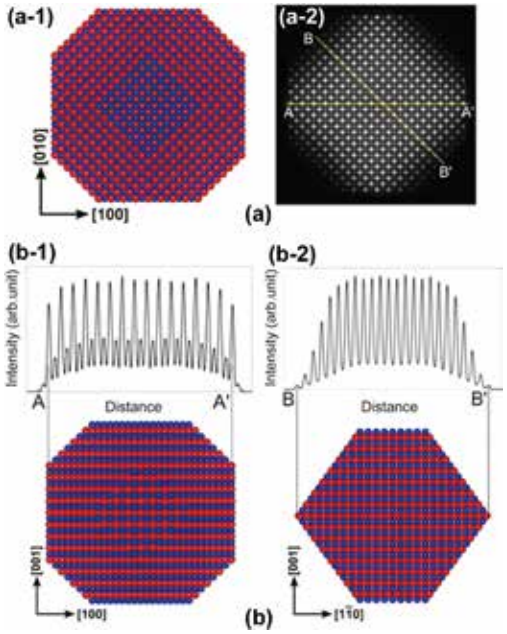

Fig. 2 (a) A truncated octahedron composed of 8000 atoms and a simulated HAADF-STEM image. (b) Intensity profiles of simulated images measured in the [100] (b-1) and [1$\bar{1}$0] (b-2).

Figure 1(b) shows a *Z*-contrast image of a CoPt NP composed of three-variant ordered domains. The NP contains (001) facets, and therefore, an alternating stacking of (001) planes of Co and Pt can be directly distinguished. They are both terminated by Co atoms as indicated by arrowheads though Pt termination was predicted by theoretical simulations. This discrepancy suggests that the NP shown in Fig. 1(b) may not be in thermodynamic equilibrium, as indicated by the multiple domains present.

In summary, we demonstrated that a large *Z* difference enables intuitive interpretation of atomic ordering in bimetallic NPs due to the incoherent nature of *Z*-contrast imaging.

References

[1] K. Sato, T. J. Konno, and Y. Hirotsu, Advances in Imaging and Electron Physics **170**, 165 (2012).

[2] F. Tournus, K. Sato *et al.*, Phys. Rev. Lett. **110**, 055501 (2013) / ibid. **110**, 087207 (2013).

[3] K. Sato *et al.*, J. Nanomater. **2013**, 679638 (2013).

Keywords: scanning transmission electron microscopy (STEM), nanoparticle, ordering
Kazuhisa Sato (Materials Science of Non-Stoichiometric Compounds Division)
E-mail: ksato@imr.tohoku.ac.jp
URL: http://konno-lab.imr.tohoku.ac.jp

Spin correlation in the frustrated spin chain system of $CuGeO_3$

$CuGeO_3$ is a unique quantum spin system that undergoes the spin-Peierls transition at 14 K. In order to study spin correlations in $CuGeO_3$, we investigated the temperature dependence of the entire spin excitation by high-energy neutron scattering. The results can be explained on the basis of the deformation of a spin dimer caused by thermal disturbance while retaining a large frustration between antiferromagnetic first and second nearest neighbor couplings.

In the research on spin correlations in complex magnetic systems, studies of perturbations by impurities [1], magnetic fields, and lattice distortion [2] on the overall magnetism are effective approaches. $CuGeO_3$ is the first known inorganic spin-Peierls (SP) compound. However, the mechanism of the SP transition is still under debate, since the phonon softening corresponding to the lattice distortion has not been detected. In order to shed more light on this issue, we studied the thermal evolution of spin excitation, which reflects the origin of spin correlation, by means of time-of-flight high-energy neutron scattering techniques.

As shown in Fig. 1, the intensity hump on the upper boundary of the continuum excitation was observed at low temperature. Upon warming, the intensity degrades and disappears above ~90 K, whereas the outline of the continuum excitation does not change up to 180 K. (see Fig. 2) Furthermore, we found that the intensity of the lowest excited mode is strongly suppressed around the zone center (ZC), while it persists around the zone boundary (ZB). The existence of the intensity hump is consistent with the theoretical result for the frustrated spin chain with a large competition rate between the first- and second-nearest neighbor exchange couplings. Therefore, the disappearance of the intensity hump at high temperature indicates the thermal deformation of a spin dimer, which is stabilized through spin frustration at low temperatures. The identical temperature dependence of the magnetic intensity at the ZC and ZB suggests that the spin correlation is spatially confined to a limited range [3].

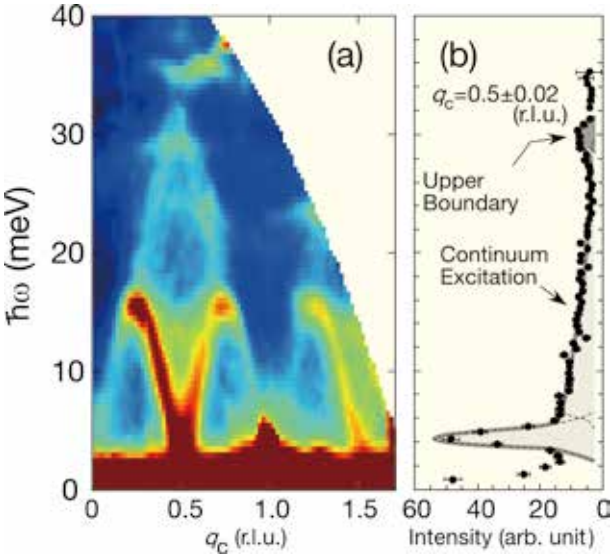

Fig. 1 (a) Entire spin excitation, and (b) the constant-q_c spectrum at q_c = 0.5 along the energy direction.

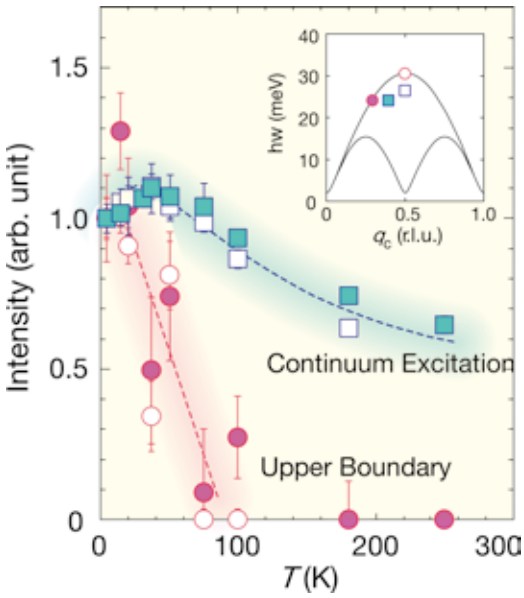

Fig. 2 Temperature dependence of the magnetic intensity measured at the upper boundary of the excitation spectrum (circles) and in the interior of the spectrum (squares).

References

[1] M. Fujita, M. Enoki, K. Tsutsumi, S. Iikubo, and K. Yamada, J. Korean. Phys. Soc. **62**, 1840 (2013).

[2] M. Enoki, M. Fujita, and K. Yamada, Phys. Soc. Jpn. **82**, 114707 (2013).

[3] M. Fujita, C. D. Frost, S. M. Bennington, R. Kajimoto, M. Nakamura, Y. Inamura, F. Mizuno, K. Ikeuchi, and M. Arai, J. Phys. Soc. Jpn. **82**, 084708 (2013).

Keywords: spin excitation, neutron scattering
Masaki Fujita (Materials Processing and Characterization Division)
E-mail: fujita@imr.tohoku.ac.jp
URL: http://qblab.imr.tohoku.ac.jp